Hierarchically mesostructured porous TiO_2 hollow nanofibers for high performance glucose biosensing

Qiaohui guo, Lijuan Liu, Man Zhang, Haoqing Hou, Yonghai Song, Huadong Wang, Baoying Zhong, Li Wang

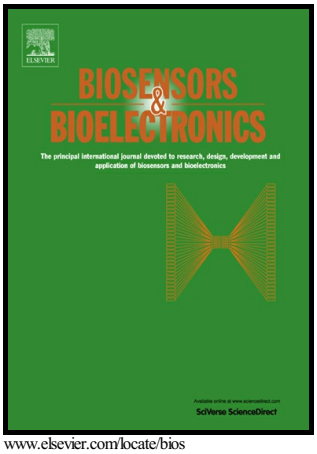

www.elsevier.com/locate/bios

PII: S0956-5663(16)31059-4
DOI: http://dx.doi.org/10.1016/j.bios.2016.10.036
Reference: BIOS9258

To appear in: *Biosensors and Bioelectronic*

Received date: 2 August 2016
Revised date: 1 October 2016
Accepted date: 18 October 2016

Cite this article as: Qiaohui guo, Lijuan Liu, Man Zhang, Haoqing Hou, Yongha Song, Huadong Wang, Baoying Zhong and Li Wang, Hierarchically mesostructured porous TiO_2 hollow nanofibers for high performance glucos biosensing, *Biosensors and Bioelectronic* http://dx.doi.org/10.1016/j.bios.2016.10.036

Hierarchically mesostructured porous TiO_2 hollow nanofibers for high performance glucose biosensing

Qiaohui guo*, Lijuan Liu, Man Zhang, Haoqing Hou, Yonghai Song, Huadong Wang, Baoying Zhong, Li Wang*

Department of Chemistry and Chemical Engineering, Jiangxi Normal University, Nanchang; Jiangxi 330022, China

*Corresponding Author: Qiaohui Guo, Ph.D.

Tel: (+86) 791-8812-0389; Fax: (+86) 791-8812-0536

E-mail address:guoqiaohui@jxnu.edu.cn

Abstract

Effective immobilization of enzymes on an electrode surface is of great importance for biosensor development, but it still remains challenging because enzymes tend to denaturation and/or form close-packed structures. In this work, a free-standing TiO_2 hollow nanofibers (HNF-TiO_2) was successfully prepared by a simple and scalable electrospun nanofiber film template-assisted sol-gel method, and was further explored for glucose oxidase (GOD) immobilization and biosensing. This porous and nanotubular HNF-TiO_2 provides a well-defined hierarchical nanostructure for GOD loading, and the fine TiO_2 nanocrystals facilitate direct electron transfer from GOD to the electrode, also the strong interaction between GOD and HNF-TiO_2 greatly enhances the stability of the biosensor. The as-prepared glucose biosensors show good sensing performances both in O_2-free and O_2-containg conditions with good sensitivity, satisfactory selectivity, long-term stability and sound reliability. The novel textile formation, porous and hierarchically mesostructured nature of HNF-TiO_2 with excellent analytical performances make it a superior platform for the construction of high-performance glucose biosensors.

Keywords: TiO_2 hollow nanofiber; Sol-gel method; Direct electron transfer; Glucose oxidase; Glucose biosensor.

1. Introduction

Direct electron transfer (DET) between the immobilized protein molecules and an electrode is of great significance in developing advanced bioelectrocatalytic devices and high-performance amperometric enzymatic biosensors (Beissenhirtz et al., 2004; Wei et al., 2002). However, the DET of redox protein is rarely observed on bare electrodes because the redox center of the enzyme is deeply embedded in a thick insulating protein shell. For example, FAD (flavin adenine dinucleotide)/$FADH_2$, the prosthetic group of glucose oxidase (GOD), is embedded at a depth of about 13 Å inside the insulating, and this spacing between the prosthetic group and the electrode surface generally exceeds the critical electron-tunneling distance (Guo and Li, 2010). Over the past few decades, various kinds of materials, such as carbon nanofibers (Liu et al., 2014; Zhang et al., 2015), carbon nanotubes (Goran et al., 2013; Zhang et al., 2016), graphene (Zhou et al., 2009)), metal nanoparticles (Pt, Pd and Au) (Zhu et al., 2011), and metal oxides (Wang et al., 2009) have been widely explored for the construction of high performance biosensors. Among these studies, many reports aimed at the construction of state-of-the-art electrochemical biosensors with excellent electroanalytical performance. However, the poor biocompatibility and complex chemical functionalizations of pristine carbon nanomaterials, the high-cost of noble metal nanoparticles, and relatively low electrical conductivity of metal oxides limited their practical applications.

Recently, one-dimensional (1D) TiO_2 nanostructures have attracted considerable interest in various areas such as dye-sensitized solar cells (Mor et al., 2006), photocatalysis (Mor et al., 2005), electrochromic devices (Nah et al., 2008), and lithium-ion batteries (Chen et al., 2010; Jin et al., 2016; Ren et al., 2016). Due to its excellent biocompatibility, relatively high conductivity, environmentally benign

nature, chemical and thermal stability, TiO_2 has also been extensively applied in proteins and emyzes immobilization for promising biosensor applications (Si et al., 2011; Bao et al., 2008). The electrochemical performance of TiO_2 depands not only on the crystalline structure, but also on the textural properties (e.g., dimension, geometry, porosity, and surface area) (Mor et al., 2006). In order to develop high-performance biosensors, great effort has been dedicated to synthesize various kinds of TiO_2 (e.g., nanoparticles, nanosheets, nanorods, nanotubes and so on) with a controllable morphology and pore structure. For example, Xie et al (Xie et al., 2011) synthesized a nanosheet-based TiO_2 microsphere with a hollow core-shell structure. With the unique trumpet-shaped pores on the nanosheet, the adsorbed GOD easily immobilized on the inner core of the microspheres. Kim and co-workers have prepared a novel 1D hierarchically structured TiO_2, which realized the efficient DET of GOD (Si et al., 2011).

More recently, TiO_2-based nanomaterials with free-standing structure have been attracted more and more attention in the electrocatalysis field for their unique electrochemical properties and excellent processability. In fact, previous studies have demonstrated that the free-standing TiO_2 films, such as TiO_2-graphene hybrid paper and TiO_2-carbon cloth could provide a continuous electron transport framework with lower ion transport resistance, shorter electrolyte diffusion length, and higher active material-to-substrate mass ratios in comparison with conventional nanomaterials (Hu et al., 2013; Liu et al., 2016; Ding et al., 2011). Nevertheless, there are few reports about the free-standing TiO_2 nanomaterials being used in the study of DET-based biosensors.

Template-based nanoengineering methods have been widely studied due to their simplicity, cost-effectiveness, and shape-control capabilities. Various materials such

as porous alumina (Lee et al., 2009), polystyrene spheres (Xia et al., 2009), surfactants (Peng et al., 2003), and carbon nanotubes (Si et al., 2011) have been employed to synthesize different TiO_2 nanomaterials. Electrospinning has emerged as one of the most powerful techniques for producing 1D nanofibers ranging from a few nanometers to several micrometers (Guo et al., 2014; Yang et al., 2014). The intriguing features of electrospun nanofibers, such as high porosity, large surface area, facile processability and good mechanical properties, have shown potential applications in various fields including biomedicines (Miao et al., 2012), energies (Huang et al., 2008), and environments (Guo et al., 2009). Herein, an electrospun nanofiber film (ENF) with a high specific surface area and a uniform size was used as a template to synthesize free-standing TiO_2 hollow nanofibers (HNF-TiO_2). Thereafter, GOD was integrated into the HNF-TiO_2 with a large specific surface area. This GOD/HNF-TiO_2 sensing system has several advantages and has resulted in excellent electrocatalytical performances in O_2-free and O_2-containing conditions. From the point of view of materials synthesis, ENF with a well-defined hierarchical nanofibrous structure is considered to be a perfect choice to act as bio-templates for nanomaterial fabrication. GOD could be integrated into the nanotubular HNF-TiO_2-modified electrode, and thus higher enzyme loading and good electrical contact between the enzyme and the electrode were achieved due to the unique structure of the fabricated HNF-TiO_2 material. In addition, superior sensing performances in both in O_2-free and O_2-containing conditions were achieved by this GOD/HNF-TiO_2-modified electrode, which showed many attractive analytical features, such as good sensitivity, satisfactory selectivity, long-term stability and sound reliability.

2 Results and discussion

2.1 Material Characterizations

"Here Scheme 1"

Generally, porous nanomaterial is propitious to the adsorption of enzymes and proteins, which is a vital factor affecting the performance of biosensors. Herein, a porous HNF-TiO_2 has been successfully prepared by a combination of sol-gel process and an ENF template, and the preparation process of HNF-TiO_2 was shown in Scheme 1. The ENF template can be used to control the size of HNF-TiO_2, which typically ranges from 300 to 350 nm in diameter and several micrometers in length, displaying an 1D free-standing network structure (Fig. S1). When the ENF was dipped into the TiO_2 sol, a thin layer of TiO_2 sol was encapsulated on the surface of ENF, and its diameter increased to about 500 nm with rough surface (Fig. S2). The as-expected free-standing HNF-$TiO_2$was obtained after calcining the composite at 550 ^{o}C for 2 h (Fig. 1A). The diameter of HNF-TiO_2 was about 100-150 nm with tens of micrometer in length (Fig. 1B), much smaller than the TiO_2-ENF composite, possibly because of the partial collapse of HNF-TiO_2 during the calcination process. Apparently, the size distribution of HNF-TiO_2 was largely controlled by the ENF template. Closer observation revealed a rough, porous and hollow tubular structure of the HNF-TiO_2 (Inset of Fig. 1B).

"Here Fig. 1"

Observation under TEM measurements further revealed the porously hollow nature of HNF-TiO_2. As shown in Fig.1C, D, the hollow structured HNF-TiO_2 possessed good uniformity and conformability as well as high porosity, and its wall thickness was about 50 nm. Such rough and hollowed structure was especially beneficial for the high accessibility of target molecules to the device surface and the

stabilization of the immobilizated biomaterials, especially in the case of enzyme. To get more insight into the morphology and compositional homogeneity, the HNF-TiO_2 was subjected to HRTEM and SAED analyses. It was evident from the representative HRTEM image (Fig. 1E) that the HNF-TiO_2 consisted of lots of nanocrystals arranged and showed a polycrystalline structure. The interplanar distance of the fringes was 0.33 nm, corresponding to the (101) facet of anatase TiO_2. SAED pattern further indicated the nanocrystal structure of HNF-TiO_2 (Fig. 1F), which showed continuous rings referred to the single-phase anatase TiO_2. The continuity of the ring indicated that the HNF-TiO_2 was polycrystalline. The diffraction rings can be indexed to the (101), (004), (200), (105) and (211) facets of anatase TiO_2, respectively. The above results strongly supported that the proposed approach was a desirable process for the fabrication of free-standing and porous anatase HNF-TiO_2.

"Here Fig. 2"

The crystal structure of HNF-TiO_2 was also determined by XRD. As shown in Fig. 2A, the main peaks at 25.6, 38.5, 49.0, 54.4 and 55.6^o corresponded to the (101), (004), (200), (105) and (211) crystal facets of anatase TiO_2, respectively (JCPDS No. 21-1272), indicating that HNF-TiO_2 was in an anatase structure, which was in agreement with the SAED findings. No other impurities were detected, reflecting the high purity and high crystallinity of the resultant HNF-TiO_2 sample. Raman spectrum exhibited five mains at 144, 197, 400, 519 and 640 cm^{-1}, corresponding to the E_g and B_{1g} of anatase TiO_2 (Fig. S3A). The chemical composition of the HNF-TiO_2 was investigated by EDX, showing strong Ti and O signals (Fig. S3B), confirming the phase purity of HNF-TiO_2. These results proved the successful formation of anatase HNF-TiO_2 with high crystallinity and high purity, which was consistent with the HRTEM and SAED results.

The nitrogen adsorption/desorption isotherm curves demonstrated type-IV isotherm (Fig. 2B), which has a sharp capillary condensation step at relative high pressures, implying the presence of porous structure and a narrow distribution of pore sizes, consistenting with the SEM and TEM analyses. The calculated specific surface area of HNF-TiO_2 was 165.2 m^2 g^{-1}. The enlarged surface area provided abundant active sites for the immobilization of enzymes, hence the porous HNF-TiO_2 sample was expected to be a idea material in the detection of electroactive species. The pore size distribution was calculated by the BJH method (Insert of Fig. 2B). It can be seen that the pore diameter of the HNF-TiO_2 sample was mainly distributed at around 6-9 nm with large pore volume, roughly matching the dimension of GOD molecules (7.0 nm×5.5 nm×8.0 nm) (Hartmann, 2005). A high surface area and a uniform pore distribution are especially beneficial for TiO_2-based sensing because these properties promote the interaction between biomolecules and material and allow for high accessibility of target molecules to the electrode surface (Walcarius, 2011).

3.2 Immobilization of GOD on HNF-TiO_2

On the basis of above results, it is interesting found that a free-standing HNF-TiO_2 could be facilely fabricated by a combination of ENF template-assisted sol-gel process, possessing large surface area, narrow size distribution, good uniformity and conformability as well as high porosity, which was fairly favorable for enzyme immobilization and further the construction of highly sensitive and stable biosensors. To demonstrate the practical utility of HNF-TiO_2, a GOD was chosen as a model to evaluate the sensing performance.

"Here Fig. 3"

Firstly, the effectiveness of GOD immobilization on HNF-TiO_2 was investigated. Various studies indicated that the denaturation of GOD upon its absorption on the

nanostructured surface and the loss of enzyme was usually related to the change of GOD structure (Seehuber and Dahint, 2011), the immobilized GOD on the HNF-TiO_2 was examined by FT-IR, UV-vis spectra and EIS technique, efficient tools to study the bioactivity-related secondary structure of enzyme. The pure GOD exhibit two characteristic peaks at 1650 and 1543 cm^{-1}, corresponding to the typical amide I and amide II adsorption bands of proteins (Fig. 3A) (Wu et al., 2007). The signal peak at 1095 cm^{-1} was attributed to the C-O bond stretching vibration of GOD (Bao et al., 2008). The HNF-TiO_2 has bands at 1636 and 1035 cm^{-1}, which were ascribed to the deformational vibration of the H-O-H bond from absorbed water (Guo and Li, 2010). The amide adsorption peaks are generally used as an indication of protein denaturation and conformational change upon immobilization. The presence of both amide I and II adsorption peaks in the spectrum of GOD-loaded HNF-TiO_2 indicated that the enzyme retained its activity after being adsorbed on the surface of HNF-TiO_2. The amide adsorption peaks were downshifted slightly to 1640 and 1526 cm^{-1}, possibly due to the strong electrostatic interaction between the anchored enzyme and the HNF-TiO_2, since GOD is negatively charged in a neutral solution (isoelectric point = 4.2) (Liu et al., 2014), while HNF-TiO_2 is positively charged in a neutral solution due to its relatively high isoelectric point (Si et al., 2011). On the other hands, as well-known, Fourier Transform infrared (FT-IR) spectroscopy in the amide I region coupled with proper deconvolution procedures is considered one of the most useful tools for investigating the secondary structure of proteins and for monitoring the enzyme activity (Kamilya et al., 2009). Herein, enzyme structure was determined by curve fitting the amide I band (1580-1700 cm^{-1}) into its respective secondary structure components (Fig. 3B and Fig. S4). The results indicated that enzymatic activity of GOD was preserved and a predominant β-sheet subcomponent is retained

for GOD adsorbed on the HNF-TiO_2 surface. Additionally, UV-vis results further indicated that the GOD immobilized in HNF-TiO_2 maintained its native structure (Fig. S5).

EIS technique was also used to monitor the fabricating process. The electron transfer kinetics of $[Fe(CN)_6]^{3-/4-}$ redox couple at different modified electrodes was shown in Fig. 3C. The HNF-TiO_2 modified electrode exhibited a lower electron transfer resistance (R_{ct}) in comparison with the bare GC, indicating that HNF-TiO_2 had high electrical conductivity. Nevertheless, the R_{ct} of GOD/HNF-TiO_2 was greater than that of HNF-TiO_2. The reason was due to the immobilized protein formed an insulating barrier to electron transfer. This result further confirmed that the GOD has successfully immobilized on the HNF-TiO_2 surface. Additionally, the surface coverage of GOD (Θ) on the electrode surface can be derived according to the equation (Liu et al., 2007): $\Theta = 1 - R_{ct}/R_{ct}^{GOD}$, where R_{ct} is the charge transfer resistance of the HNF-TiO_2 modified electrode, and R_{ct}^{GOD} is the corresponding resistance of GOD/HNF-TiO_2 modified electrode, and the calculated Θ was 99.2%. Such a high surface coverage of enzyme could contribute to the superior enzyme loading capability of HNF-TiO_2 as a result of its large surface area, mesoporous and hollow tubular structure, and positive surface charge.

3.3 Direct Electrochemistry and Bioelectrocatalysis of GOD in O_2-Free Solution

To study the DET of GOD immobilized on HNF-TiO_2, CV measurements were performed in 0.1 M O_2-free PBS solution (pH 7.0). It was noticeable that a pair of well-defined redox peaks with anodic (E_{pa}) and cathodic (E_{pc}) of -0.427 and -0.448 V could be observed at GOD/HNF-TiO_2/GC electrode (Fig. 3D), consistenting with the typical electrochemical characteristics of GOD (Song et al., 2016), indicating that the redox center of GOD immobilized on HNF-TiO_2 was a quasi-reversible reaction as:

$FAD + 2H^+ + 2e^- \leftrightarrow FADH_2$ (Goran et al., 2013). The peak-to-peak separation ($\Delta E_p = E_{pa} - E_{pc}$) was around 21 mV, much smaller than that of other TiO_2-based electrodes, e.g., mesoporous TiO_2 (58 mV) (Bao et al., 2008), hierarchically structured TiO_2 (38 mV) (Si et al., 2011), hierarchical TiO_2 nanosheets array/carbon cloth (34 mV) (Liu et al., 2016), indicating a significantly increased electron transfer rate and enhanced reversibility of the redox reaction. The control experiments of HNF-TiO_2/GC, GOD/GC electrodes showed no obvious response, indicating that the presence of both GOD and HNF-TiO_2 on the electrode surface was necessary to obtain the typical current response.

Laviron's model is widely used to estimate the heterogeneous electron-transfer rate constant (k_s) for electrochemical reactions (Laviron, 1979).The k_s of GOD immobilized on HNF-TiO_2 was calculated to be 8.6 s^{-1}, which was larger than those of GOD immobilized on hierarchical TiO_2 (7.8 s^{-1}) (Si et al., 2011), mesoporous TiO_2 (3.96 s^{-1}) (Bao et al., 2008), PEDOT-NiO (3.12 s^{-1}) (Guo and Li, 2010) and nitrogen-doped CNT (7.6 s^{-1}) (Goran et al., 2013). This result indicated that the HNF-TiO_2 could enhance the DET between the redox active sites of GOD and electrode owing to the strong interaction between HNF-TiO_2 and GOD, the effective loading of GOD, and their relatively high electrical conductivity. In addition, the surface coverage (Γ) of GOD/HNF-TiO_2 was calculated to be 9.68×10^{-10} mol cm^{-2}, a value that was much greater than that of mesoporous TiO_2 (2.57×10^{-10} mol cm^{-2}) (Bao et al., 2008), hierarchically structured TiO_2 (6.86×10^{-10} mol cm^{-2}) (Si et al., 2011) and Au NPs (9.8×10^{-12} mol cm^{-2}) (Liu and Ju, 2003).

The electrochemical response of GOD/HNF-TiO_2 also displayed strong dependence on the scanning rate (Fig. S6) and solution pH value (Fig. S7), showing that the redox reaction of $FAD/FADH_2$ in the active center of GOD was a surface-

controlled with a two-electron coupled a two-proton electrochemical process. Apparently, the fast electron transfer rate and the excellent biomolecule immobilization capacity of the porous HNF-TiO_2 offered great advantages to fabricate biosensors, which was very important in bioanalysis and clinical applications.

To study glucose oxidation on GOD/HNF-TiO_2/GC electrode, CV measurements was carried out in a O_2-free PBS solution containing different concentrations of glucose. A pair of well-defined redox peaks was observed in the absence of glucose due to the reversible reaction of FAD/$FADH_2$. While increasing in the glucose concentration, both the anodic and cathodic peak currents decreased (Fig. 4A). The mechanism of glucose oxidation in O_2-free condition based on TiO_2 nanomaterials was proposed by Kim and co-workers (Si et al., 2011). They suggested that the FAD at the redox center of GOD immobilized on TiO_2 was directly involved in the glucose oxidation reaction without any mediator, and as glucose concentration increased, GOD(FAD) was increasingly converted into GOD($FADH_2$), leading to a continuous decrease in the cathodic and corresponding anodic peak currents. Herein, the mechanism of glucose oxidation in O_2-free condition was not very clear, and need to further study. The glucose detected in O_2-free PBS solution displayed a linear range of 0.006-1.5 mM (R = 0.997) (Fig. 4B) with a sensitivity of 22.5 μA mM^{-1} cm^{-2}, and a detection limit (LOD) of 2 μM (S/N=3). For comparation, we also investigated the CVs of FAD/HNF-TiO_2/GC in O_2-free PBS solution without and with 1 mM glucose (Fig. 4C). The addition of glucose displayed no effect on the peak current of FAD/HNF-TiO_2/GC, indicating that the FAD was only the electroactive but not the enzymatically active of GOD.

"Here Fig. 4"

The stability of the GOD/HNF-TiO_2/GC biosensor in O_2-free condition was

investigated, and the result was shown in Fig. S8A. After two weeks, the catalytic current response of 1.0 mM glucose only decreased by 2.5%, demonstrating the good stability. For evaluation of the electrode-to-electrode reproducibility, six GOD/HNF-TiO_2/GC sensors were prepared in the same way. The responses of the six sensors toward 1.0 mM glucose showed a RSD of 4.3% (Fig. S8B). The selectivity of the GOD/HNF-TiO_2/GC sensor was also studied. Fig. 4D presented the catalytic current response of the sensor to 1.0 mM glucose, including a 0.1 mM of interfering substances, such as some sugars, UA, AA, and DA. Compared to glucose, the current responses were 1.54%, 0.75%, 0.78%, 0.77%, 1.23%, 1.85% and 1.15% for AA, DA, UA, xylose, mannose, maltose and lactose, respectively, indicating a high selectivity of the fabricated sensor. The good stability, reproducibility and selectivity of the GOD/HNF-TiO_2/GC made it a promise material for the construction of glucose biosensors.

3.4 Bioelectrocatalysis of GOD in O_2-Containing Solution

Similar CV measurements were conducted in air-, O_2-saturated PBS solution (Fig. 5A). Compared with the CV in O_2-free condition, an obvious cathodic current was observed at a potential of less than -0.4 V in air-saturated PBS solution, and the peak current became larger in O_2-saturated PBS solution. The results confirmed that the dissolved oxygen in the solution was catalytically reduced at the modified electrode. More importantly, when glucose was added into the air-saturated PBS, a significant decrease of O_2 reduction peak current was observed (Fig. 5B), which may be ascribed to the consumption of O_2 from the naturally enzymatic glucose oxidation. Herein, the bioelectrocatalytic process of GOD toward glucose was different from that in O_2-free solution, where glucose was oxidized by GOD(FAD) into glucono-1,5-lactone and oxygen was reduced by GOD($FADH_2$) to H_2O_2 (Wooten et al., 2014):

$$\text{glucose} + \text{GOD(FAD)} \longrightarrow \text{glucono-1,5-lactone} + \text{GOD(FADH}_2\text{)}$$

$$\text{GOD(FADH}_2\text{)} + \text{O}_2 \longrightarrow \text{GOD(FAD)} + \text{H}_2\text{O}_2$$

Considering GOD could catalyze glucose into gluconolactone accompanied by the reduction of oxygen, glucose thus could be quantitatively detected the amount of oxygen consumed in the reduction.

"Here Fig. 5"

The glucose sensing performance of the GOD/HNF-TiO_2/GC electrode was evaluated by amperometric measurement in air-saturated PBS solution. As shown in Fig. 5C, D, strong and fast response with 95% of the steady-state current could be achieved within 3 s at GOD/HNF-TiO_2/GC. Under O_2-containing condition, the glucose biosensor showed a wide linear range of 0.002 to 3.17 mM (R = 0.998) with a LOD of 0.8 μM (S/N = 3) and a sensitivity of 32.6 μA $mM^{-1}cm^{-2}$. The linear range of glucose biosensing in air-saturated PBS was wider than that in O_2-free PBS, suggesting that O_2 was also involved in the biosensing process. A detailed comparison between the GOD/HNF-TiO_2/GC and other GOD-based glucose sensors was listed in Table S1. By comparison, the GOD/HNF-TiO_2/GC biosensor offered a reasonable sensitivity, a low LOD, and a wide linear range. The remarkably improved electrochemical performance of GOD/HNF-TiO_2/GC could be attributed to several factors. First, the immobilized GOD could enter into the pores of HNF-TiO_2 due to the similarity in their sizes, significantly shortening the electron tunneling distance between the enzyme's active center and HNF-TiO_2. Second, the strong electrostatic interaction between GOD and HNF-TiO_2 could further narrow the spacing between the material and the adsorbed enzyme, facilitating the electron transfer between the electrode and immobilized GOD molecules. Third, the great biocompatibility of HNF-TiO_2 for maintaining the bioactivity of GOD, which was favorable for the direct

electrochemical reaction. Finally, due to the unique network and hollow tubular structure of the porous HNF-TiO_2, on which a large number of GODs could efficient immobilized inner and on the surface of HNF-TiO_2, and hence enlarge the specific surface area.

Another attractive feature of GOD/HNF-TiO_2/GC sensor in O_2-saturated solution was the excellent reproducibility and stability. The batch-to-batch reproducibility of the as-fabricated sensor was estimated from the current responses of six different sensors to 2.0 mM glucose, and the RSD was 4.8 %. In addition, the sensor showed high reproducibility toward the detection of 1.0 mM glucose with a RSD of 3.6 % for ten continuous assays (Fig. S9). When the sensor was stored at 4 ^{o}C for 2 weeks, the fabricated biosensor remained 95.7 % of its bioactivity (Fig. S10). The good stability during the measurements and the long lifetime of the biosensor attributed to its ability to strongly entrap GOD molecules and good biocompatibility of the porous HNF-TiO_2 for retaining their biological activity and strong affinitive association between GOD and HNF-TiO_2.

The selectivity of the GOD/HNF-TiO_2/GC biosensor was also studied. The addition of AA, DA, UA and some sugars did not cause obvious current signal for glucose (Fig. S11), suggesting that the proposed sensor can be used to selectively detect glucose. The detection of glucose in blood serum samples indicated that the biosensor performs very well (Table S2). The results indicated that the GOD/HNF-TiO_2/GC sensor was stable enough to detect glucose selectively in a practical sample.

3. Conclusions

This work reported a simple and effective method to fabricate free-standing, porous HNF-TiO_2 with a large specific surface area and uniform pore distribution. The HNF-TiO_2 was easily synthesized by using an ENF-assisted sol-gel method. Experimental results demonstrated that the HNF-TiO_2 was an attractive matrix to immobilize enzyme and exhibited facile, direct electrochemistry of GOD. The great biocompatibility of HNF-TiO_2 and the strong electrostatic interaction between GOD and HNF-TiO_2 contributed to the high bioactivity of the immobilized enzyme. The glucose sensing was demonstrated in both O_2-free and O_2-saturated PBS solution, which displayed good sensitivity, satisfactory selectivity, long-term stability and sound reliability. This novel material may have potential applications in lithium ion batteries, optoelectronic devices and solar energy applications.

Acknowledgements

This work was financially supported by National Natural Science Foundation of China (21165010, 21465014, 21405065 and 21465015), the State Key Laboratory of Electroanalytical Chemistry (SKLEAC201310), Young Scientist Foundation of Jiangxi Province (20112BCB23006 and 20122BCB23011), Foundation of Jiangxi Educational Committee (GJJ13244) and Natural Science Foundation of Jiangxi Province (20142BAB203010 and 20143ACB21016), The Ministry of Education by the Specialized Research Fund for the Doctoral Program of Higher Education (20133604110002).

References

Bao, S.J., Li, C., Zang, J.F., Cui, X.Q., Qiao, Y., Guo, J., 2008. Adv. Funct. Mater. 18, 591–599.

Beissenhirtz, M.K., Scheller, F.W., Stocklein, W.F.M., Kurth, D.G., Mohwald, H., Lisdat, F., 2004. Angew. Chem. Int. Ed. 43, 4357–4360.

Chen, J.S., Tan, Y.L., Li, C.M., Cheah, Y.L., Luan, D., Madhavi, S., Boey, F.Y.C., Archer, L.A., Lou, X.W., 2010. J. Am. Chem. Soc. 132, 6124–6130.

Ding, S.J., Chen, J.S., Luan, D., Boey, F.Y.C., Madhavi, S., Lou, X.W., 2011. Chem. Commun. 47, 5780–5782.

Goran, J.M., Mantilla, S.M., Stevenson, K.J., 2013. Anal. Chem. 85, 1571–1581.

Goran, J.M., Stevenson, K.J., 2013. Langmuir 29, 13605–13613.

Guo, C.X., Li, C.M., 2010. Phys. Chem. Chem. Phys. 12, 12153–12159.

Guo, Q.H., Liu, D., Zhang, X.P., Li, L.B., Hou, H.Q., Niwa, O., You, T.Y., 2014. Anal. Chem. 86, 5898–5905.

Guo, Q.H., Zhou, X.P., Li, X.Y., Chen, S.L., Seema, A., Greiner, A., Hou, H.Q., 2009. J. Mater. Chem. 19, 2810–2816.

Hartmann, M., 2005. Chem. Mater. 17, 4577–4593.

Hu, T., Sun, X., Sun, H.T., Yu, M.P., Lu, F.Y., Liu, C.S., Lian, J., 2013. Carbon 51, 322−326.

Huang, J.S., Wang, D.W., Hou, H.Q., You, T.Y., 2008. Adv. Funct. Mater. 18, 441–446.

Jin, J., Ren, X., Lu, Y., Zheng, X., Wang, H., Chen, L., Yang, X., Li, X., Su, B., 2016. RSC Adv. 6, 70485–70492.

Kamilya, T., Pal, P., Mahato, M., Talapatra, G.B., 2009. J. Phys. Chem. B 113, 5128–5135.

Lad, U., Kale, G.M., Bryaskova, R., 2013. Anal. Chem. 85, 6349–6355.

Laviron, E., 1979. J. Electroanal. Chem. 101, 19–28.

Lee, H.O., Kim, E.M., Yu, H., Jung, J.S., Chae, W.S., 2009. Nanotechnology 20, 325604–325609.

Liu, D., Zhang, X.P., You, T.Y., 2014. ACS Appl. Mater. Interfaces 6, 6275–6280.

Liu, H.Q., Tian, Y., Deng, Z.F., 2007. Langmuir 23, 9487–9494.

Liu, J., He, Z.M., Khoo, S.Y., Tan, T.T.Y., 2016. Biosens. Bioelectron. 77, 942–949.

Liu, S.Q., Ju, H.X., 2003. Biosens. Bioelectron. 19, 177–183.

Mani, V., Devadas, B., Chen, S.M., 2013. Biosens. Bioelectron. 41, 309–315.

Miao, Y.E., Wang, R.Y., Chen, D., Liu, Z.Y., Liu, T.X., 2012. ACS Appl. Mater. Inter. 4, 5353–5359.

Mor, G.K., Shankar, K., Paulose, M., Varghese, O.K., Grimes, C.A., 2005. Nano Lett. 5, 191–195.

Mor, G.K., Shankar, K., Paulose, M., Varghese, O.K., Grimes, C.A., 2006. Nano Lett. 6, 215–218.

Nah, Y.C., Ghicov, A., Kim, D., Berger, S., Schmuki, P., 2008. J. Am. Chem. Soc. 130, 16154–16155.

Peng, T.Y., Hasegawa, A., Qiu, J.R., Hirao, K., 2003. Chem. Mater. 15, 2011-2016.

Ren, H., Sun, J., Yu, J., Yang, M., Gu, L., Liu, P., Zhao, H., Kisailus, D., Wang, D., 2016. Chem. Sci. 7, 793–798.

Shan, C.S., Yang, H.F., Han, D.X., Zhang, Q.X., Ivaska, A., Niu, L., 2010. Biosens. Bioelectron. 25, 1070–1074.

Seehuber, A., Dahint, R., 2013. J. Phys. Chem. B 117, 6980–6989.

Si, P., Ding, S.J., Yuan, J., Lou, X.W., Kim, D.H., 2011. ACS Nano 5, 7617–7626.

Song, Y.H., Lu, X.P., Li, Y., Guo, Q.H., Chen, S.L., Mao, L.Q., Hou, H.Q., Wang, L., 2016. Anal. Chem. 88, 1371–1377.

Wang, J., 2008. Chem. Rev. 108, 814–825.

Walcarius, A., 2013. Chem. Soc. Rev. 42, 4098–4140.

Wang, Z.Y., Liu, S.N., Wu, P., Cai, C.X., 2009. Anal. Chem. 81, 1638–1645.

Wei, J.J., Liu, H.Y., Dick, A.R., Yamamoto, H., He, Y.F., Waldeck, D.H., 2002. J. Am. Chem. Soc. 124, 9591–9599.

Wooten, M., Karra, S., Zhang, M.G., Gorski, W., 2014. Anal. Chem. 86, 752–757.

Wu, P., He, Y., Wang, H.F., Yan, X.P., 2010. Anal. Chem. 82, 1427–1433.

Wu, S., Ju, H.X., Liu, Y., 2007. Adv. Funct. Mater. 17, 585–592.

Xia, X.H., Tu, J.P., Zhang, J., Xiang, J.Y., Wang, X.L., Zhao, X.B., 2009. ACS Appl. Mater. Interfaces 2, 186–192.

Xie, Q., Zhao, Y., Chen, X., Liu, H., Evans, D.G., Yang, W., 2011. Biomaterials 32, 6588–6594.

Yang, G., Kampstra, K.L., Abidian, M.R., 2014. Adv. Mater. 26, 4954–4960.

Zhang, M., Zhou, G.Y., Feng, Y., Xiong, T.R., Hou, H.Q., Guo, Q.H., 2016. Sens. Actuators B 222, 829–838.

Zhang, X.P., Liu, D., Li, L.B., You, T.Y., 2015. Sci. Rep. 5, 1–6.

Zhao, S., Zhang, K., Bai, Y., Yang, W.W., Sun, C.Q., 2006. Bioelectrochemistry 69, 158–163.

Zhou, M., Zhai, Y.M., Dong, S.J., 2009. Anal. Chem. 81, 5603–5613.

Zhu, Z.H., Qu, L.N., Niu, Q.J., Zeng, Y., Sun, W., Huang, X.T., 2011. Biosens. Bioelectron. 26, 2119–2124.

Figure captions

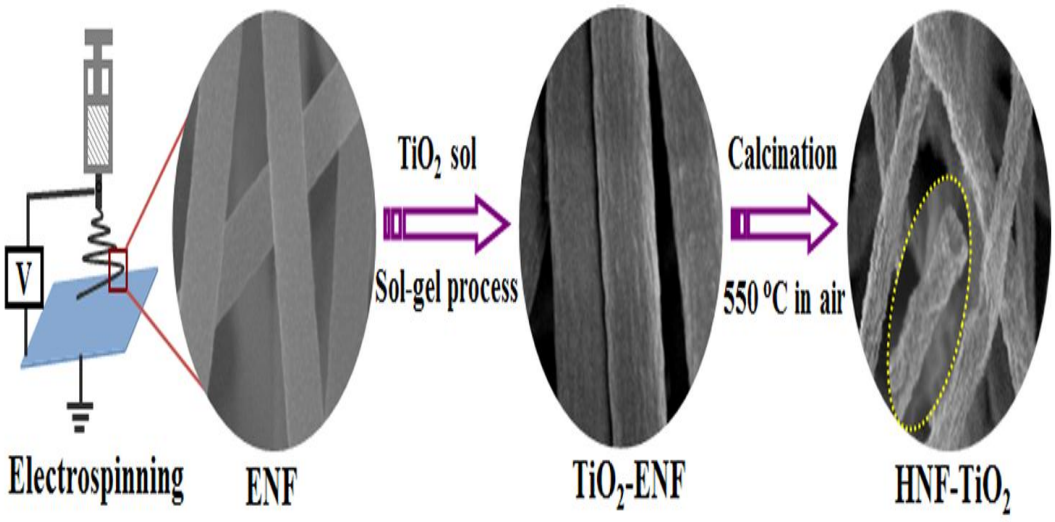

Scheme 1. Schematic illustration for the preparation of HNF-TiO_2.

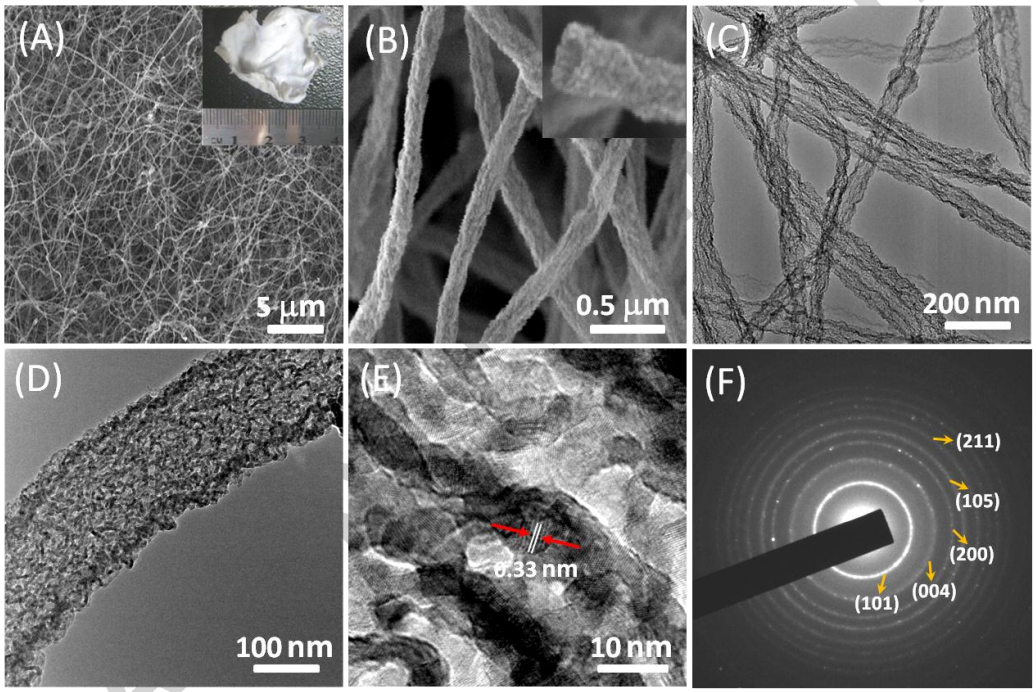

Fig.1 SEM (A, B), TEM (C, D), HRTEM (E) images and (F) SAED pattern of HNF-TiO_2. Inset of (A) and (B) are the optical photo and magnified SEM image of HNF-TiO_2, respectively.

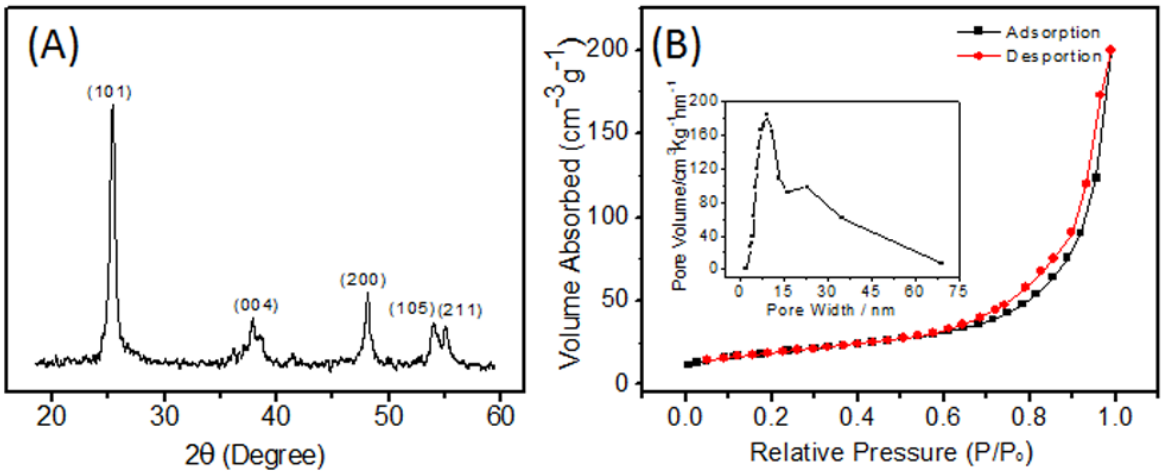

Fig. 2 XRD patterns (A) and nitrogen adsorption-desorption isotherms (B) of the HNF-TiO_2. Inset: Pore size distribution calculated from BJH method.

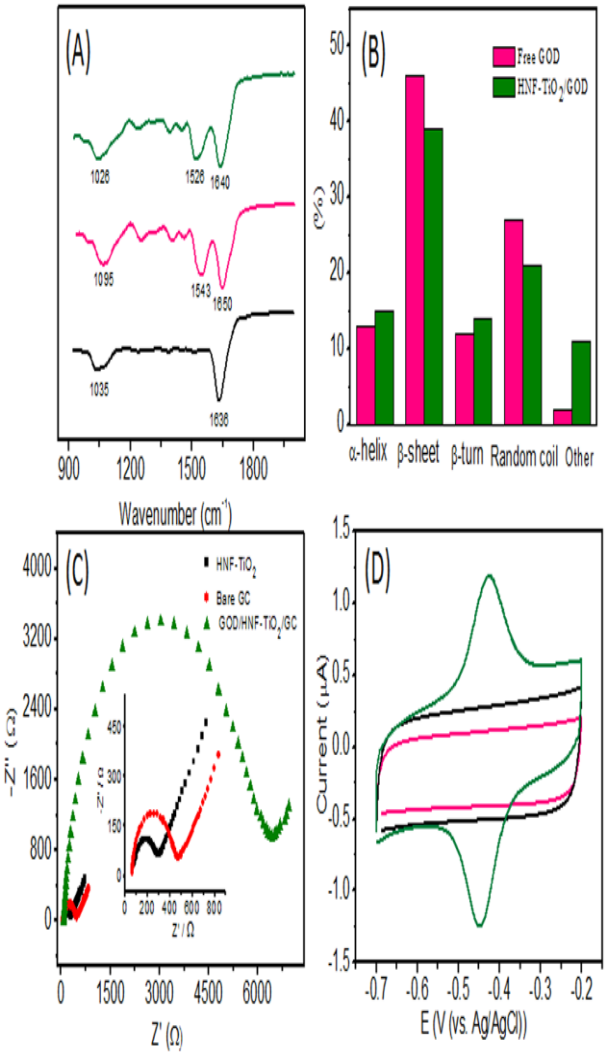

Fig. 3 (A) FT-IR spectra and CV curves (D) of HNF-TiO_2 (black), GOD (pink), and GOD/HNF-TiO_2 (green), (B) Comparison of the second structure components obtained from the value of amide I band area, (C) is the Nyquist plots of bare GC, HNF-TiO_2/GC, and GOD/HNF-TiO_2/GC, respectively.

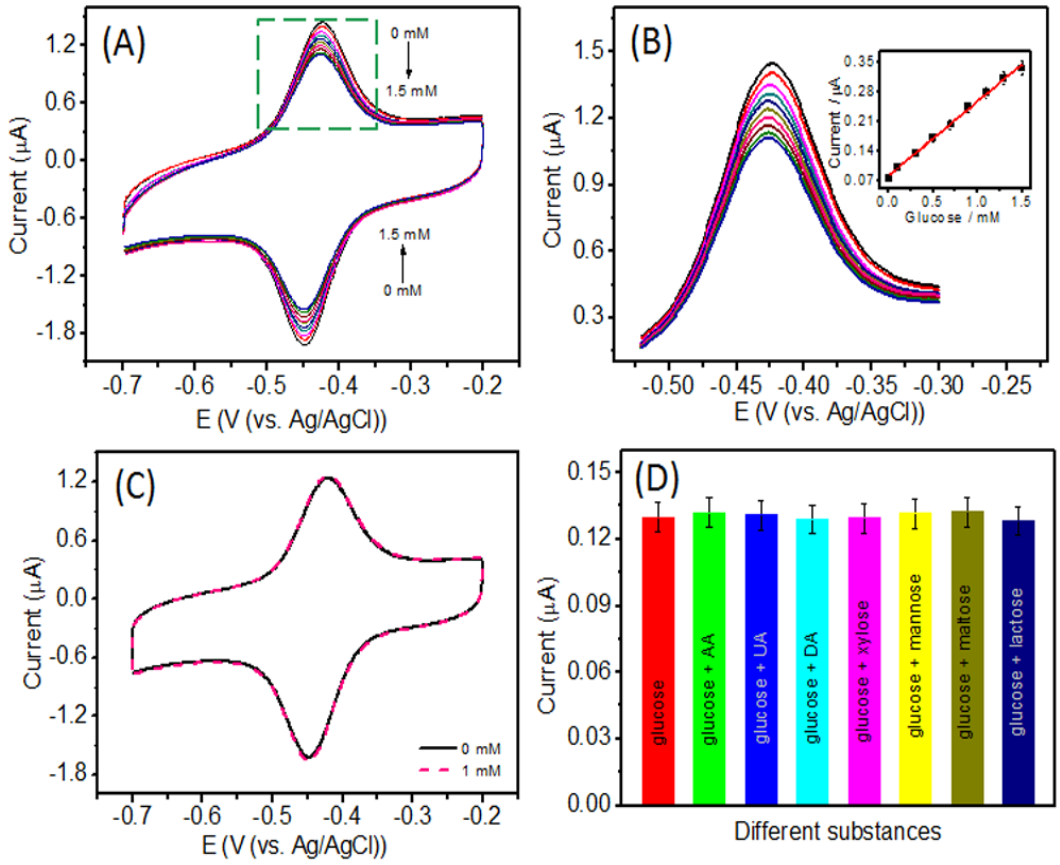

Fig. 4 (A) CV curves of GOD/HNF-TiO_2/GC in 0.1 M O_2-free PBS (pH 7.0) with different glucose concentrations. (B) The enlarged curves of the part shown in the rectangle of (A). Inset of (B) is the calibration curve. (C) CV curves of FAD/HNF-TiO_2/GC in O_2-free PBS (pH 7.0) without and with 1.0 mM glucose. Scan rate: 50 mV s^{-1}. (D) Comparison of the current for GOD/HNF-TiO_2/GC with 1.0 mM glucose and 0.1 mM other interfering substances.

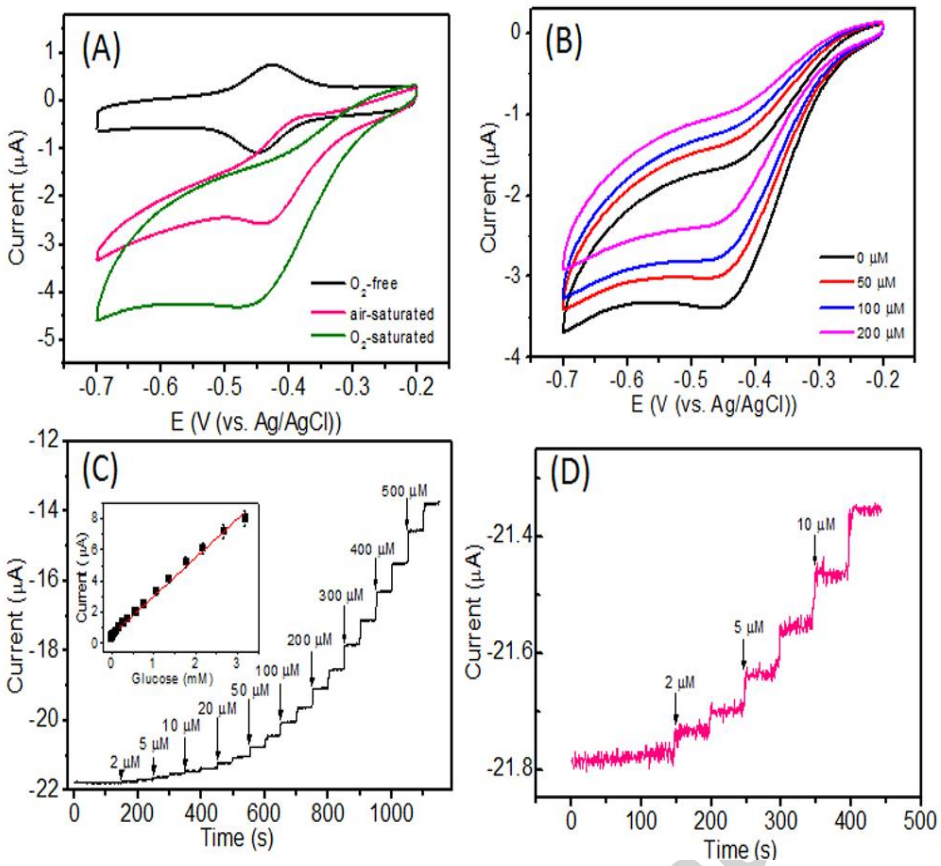

Fig. 5 CV curves of GOD/HNF-TiO_2/GC in (A) 0.1 M O_2-free, air- and O_2-saturated PBS (pH 7.0), and (B) in air-saturated PBS (pH 7.0) containing various concentrations of glucose at a scan rate of 0.05 Vs^{-1}. Current-time curves of GOD/HNF-TiO_2/GC for successive addition of various concentrations (C) and 2, 5, 10 μM (D) glucose to stirred 0.1 M air-saturated PBS (pH 7.0) at -0.45 V. Inset of (C): the calibration curve.

GRAPHICAL ABSTRACT

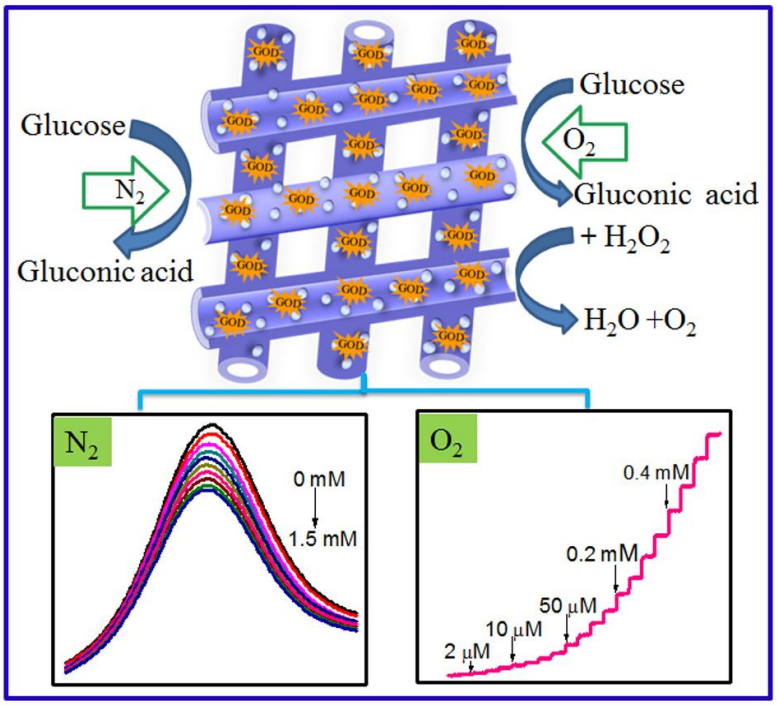

HIGHLIGHTS

1. Free-standing TiO_2 hollow nanofibers (HNF-TiO_2) was prepared by a simple and scalable electrospun nanofiber film template-assisted sol-gel method.
2. Porous and nanotubular HNF-TiO_2 provides a well-defined hierarchical nanostructure for glucose oxidase (GOD) loading.
3. The fine TiO_2 nanocrystals facilitate direct electron transfer from GOD to the electrode.

4. The strong interaction between GOD and HNF-TiO_2 greatly enhances the stability of the biosensor.
5. The as-fabricated glucose biosensors display excellent sensing performances both in O_2-free and O_2-saturated conditions.